Heliyon 10 (2024) e31676

Contents lists available at ScienceDirect

Heliyon

journal homepage: www.cell.com/heliyon

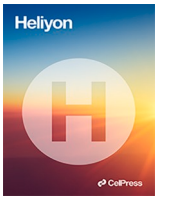

Research article

Novel ferroptosis signature for improving prediction of prognosis and indicating gene targets from single-cell level in oral squamous cell carcinoma

Zhengming Tang [a], Yuanxin Chen [a], Yisheng Huang [a], JianJiang Zhao [b,*,1], Bo Jia [a,**,1]

[a] Stomatological Hospital, School of Stomatology, Southern Medical University, Guangzhou, China
[b] Shenzhen Stomatological Hospital, Southern Medical University, Shenzhen, China

ARTICLE INFO

Keywords:
OSCC
Ferroptosis: prognostic model: bioinformatics: single-cell analysis

ABSTRACT

Background: Oral squamous cell carcinoma (OSCC) is one of the most prevalent kinds of cancers. Therefore, there is a pressing need to create a new risk scoring model to personalize the prognosis of OSCC patients and screen for patient-specific therapeutic agents and molecular targets.
Methods: Firstly, A series of bioinformatics was performed to construct a novel ferroptosis-related prognostic model; Further, drug sensitivity analysis was used to screen for specific therapeutic agents for OSCC; Single-cell analysis was employed to investigate the enrichment of FRDEGs (ferroptosis-related differentially expressed genes) in the OSCC microenvironment; Finally, various experiments were conducted to screen and validate molecular therapeutic targets for OSCC.
Results: In this study, we constructed a novel 10-FRDEGs risk scoring model. Base on the risk scoring model, we founded three potential chemotherapeutic agents for OSCC: 5Z)-7-Oxozeaenol, AT-7519, KIN001-266; In addition, FRDEGs were enriched in the epithelial cells of OSCC. Finally, we found that CA9 and CAV1 could regulate OSCC proliferation, migration and ferroptosis in vitro.
Conclusion: A novel 10-FRDEGs risk scoring model can predict the prognosis of patients with OSCC.Further,5Z)-7-Oxozeaenol, AT-7519, KIN001-266 are potential chemotherapeutic agents for OSCC.Moreover, we identified CA9、CAV1 as potential molecular target for the treatment of OSCC.Our findings provide new directions for prognostic assessment and precise treatment of oral cell squamous carcinoma.

1. Introduction

Head and neck squamous carcinoma (HNSCC) rank as the six most frequent cancer globally, with oral cancer being its predominant

* Corresponding author.
** Corresponding author.
E-mail addresses: tangzmet@163.com (Z. Tang), yuanxin_chen@yeah.net (Y. Chen), hysxuexi@163.com (Y. Huang), dentist-jia@163.com (J. Zhao), zjj2521@sina.com (B. Jia).
[1] These authors contributed equally to this work.

https://doi.org/10.1016/j.heliyon.2024.e31676
Received 7 October 2023; Received in revised form 18 May 2024; Accepted 20 May 2024
Available online 22 May 2024

subtype [1]. Oral squamous cell carcinoma (OSCC) accounted for more than 90 % of all oral cancer cases in 2018 alone, with 354,864 newly diagnosed cases and 177,384 deaths [2,3]. Despite notable advancements in modern medical interventions (e.g., surgery, radiotherapy, chemotherapy) and diagnostic techniques in recent years, the mortality rate of patients with OSCC has remained at approximately 50 % over the past decades [4].Moreover, the mortality rate continues to increase at a rate of 0.5 % per year [5]. Simultaneously, the highly heterogeneous nature of OSCC and the complex etiological mechanisms underlying the disease often render patient outcomes and survival prognosis unpredictable.

The international TNM tumor staging criteria remain the primary clinical reference for the prognosis of patients with OSCC [6]. The TNM staging criteria have continually improved, responding to the evolving body of clinical oncology research [7]. Nevertheless, several shortcomings persist in the prediction outcomes of the aforementioned approach: 1) the TNM staging criteria are based on grade information and cannot accurately assess the prognosis of patients; 2) owing to the considerable heterogeneity of tumors, tumors located in equivalent anatomical regions often exhibit varying prognostic outcomes; and 3) individual patient differences, such as familial genetic history, genetic mutations, medical histories, and previous adverse habits, are not accounted for within the criteria [7,8]. In addition, the predictive models currently utilized for the pathological grading of OSCC in clinical practice often entail the risk of tissue damage and lesion irritation [9].Therefore, there is an imperative for the development of a novel predictive model to predict the survival prognosis of patients with OSCC and also investigate the underlying biological mechanisms contributing to OSCC development, thereby improving treatment outcomes for OSCC. In recent years, the emergence of bioinformatics and transcriptome sequencing technologies has facilitated many studies elucidating that OSCC prognostic models constructed using bioinformatics techniques exhibit superior accuracy in predicting the survival prognosis of patients with OSCC and aid in the identification of therapeutic molecular targets. Thus, bioinformatics offers novel avenues for the prognostic assessment and treatment of patients with OSCC.

Ferroptosis is a unique type of programmed cell death that was identified in 2012 [10]. In ferroptosis, the primary mechanism of cell death is the accumulation of intracellular lipid peroxides mediated by iron ions, which leads to cell rupture and cell death [11,12]. Although ferroptosis is associated with apoptosis and autophagy, it differs from apoptosis, autophagy, and cell necrosis across multiple facets, including cell morphology, etiology, and regulation [13]. In addition to playing an essential role in various systemic diseases, ferroptosis, as a form of programmed cell death, assumes critical significance in the development and treatment of many malignancies [14–18]. Yang et al. showed that, in OSCC, the biological clock gene PER1 and hypoxia-inducible factor-1α together form a negative feedback loop that amplifies the regulatory influence of PER1 in ferroptosis [19].

Despite some advancements in the development of prognostic models based on ferroptosis-related genes (FRGs) with prognostic, several shortcomings still exist: 1) the limited number of FRGs in data sources used for constructing the ferroptosis-related prognostic models warrants an improvement in the accuracy of the models; 2) most of the databases used for constructing and validating the ferroptosis-related prognostic models have been restricted to single datasets (e.g., TCGA), with no utilization of external datasets (e.g., GEO) for multifaceted validation; 3) the ferroptosis-related prognostic models have not been used to explore specific therapeutic targets and strategies based on the risk grouping of patients; 4) and the expression and regulatory roles of ferroptosis-related differentially expressed genes (FRDEGs) in OSCC, which have been used to construct the ferroptosis-related prognostic models, have not been explored.

In this study, to address the shortcomings of previously established ferroptosis-related prognostic models for OSCC, we aimed to develop a novel prognostic model by conducting an in-depth investigation using bioinformatics and cell biology approaches. To this end, we used an OSCC dataset from TCGA public database and the FerrDB database to construct nomogram model for OSCC. Notably, this study is the first to investigate the expression of FRGs in OSCC at the single-cell level and subsequently corroborate these findings experimentally. Additionally, it is the first to investigate the role of CA9 and CAV1, identified as the core genes in the risk assessment model, in regulating proliferation, migration, and ferroptosis processes in OSCC. Furthermore, leveraging the ferroptosis-related prognostic model, we identified specific therapeutic agents that could improve clinical outcomes among patients with OSCC. Our research sheds new light on the function of ferroptosis and associated genes in OSCC and delineates novel avenues for prognostic assessment and treatment of patients with OSCC. Our findings show promise for improving clinical targeting strategies against OSCC and the prognosis of patients with OSCC, thereby ultimately increasing their survival rate.

2. Materials and Methods

2.1. Data sources and genetic screening

We downloaded level three HTSeq-counts data from all projects pertaining to patients with HNSCC from TCGA database. Data lacking relevant clinical information were excluded from the counts, as were those pertaining to non-oral cancer sites (e.g., lip, oropharynx, laryngopharynx, tonsils). Conversely, data pertaining to oral cancer sites were retained. Specifically, gene expression data for 329 OSCC samples and 32 paracancerous tissues were acquired from TCGA database. Furthermore, we obtained 564 FRGs from FerrDb, a database dedicated to ferroptosis research. Subsequently, the "DESeq2″ package (version 1.26.0) in R [20] was used to perform differential gene expression analysis comparing the 329 OSCC tissues with the 32 paraneoplastic tissues. Differential expression was determined based on the following criteria: gene type classified as protein_coding, $|\log2(\text{fold change})| > 1$, and p adj <0.05.

2.2. Construction of a prognostic assessment model using 10 FRDEGs

Univriate Cox regression analysis of 106 FRDEGs was performed using the "survival (version 3.2–10)" package in R. The criteria for categorizing the genes as high or low were according to the median expression level of each gene in all OSCC samples in the TCGA. In addition, The criteria for categorizing the survival of patients as good or bad were based on the height of the curves in the survival analysis. To prevent omission, we set the p value threshold of univariate cox regression analysis to 0.1. LASSO analysis of the FRDEGs was performed using the "glmnet" and "survival" packages in R, with 10-fold cross-validation and a seed number of 2021.The risk scoring model for OSCC was constructed based on the expression of the FRDEGs and their LASSO coefficients. The primary formula employed was Risk score = ni = (Coefi*xi), where "coefficient" was the coefficient of the FRDEGs following LASSO regression analysis, and "x" was the relative expression value. The patients with OSCC in database are divided into different groups based on the median risk score of after calculating by risk scoring formula.

2.3. Survival analysis and validation

We employed the "survival" and "survminer" packages and the "surv_cutpoint" function of the survminer package to determine the best cut-off values for grouping based on risk scores and to perform survival analysis. In addition, the "survival" (version 3.2–10) package was used to perform a survival analysis of TCGA data and GSE65858 pertaining to various clinical subgroups of patients with OSCC.A Decision curve analysis (DCA) of the clinicopathological features of the patients with OSCC and the 10-FRDEGs risk scoring model was performed using the "stdca" function. The clinicopathological features data of patients with OSCC from TCGA were analyzed using the "survival (3.3.1)" package in R for cox analysis. Clinicopathological characteristics such as "pathological T-stage," "pathological N-stage," "first treatment outcome," "age," and " risk scoring model risk score" were analyzed for the proportional risk hypothesis. In the case of a small number of waiting analysis variables, to prevent the omission of meaningful variables, we choose the P value threshold to be 0.1.

2.4. Development and validation of a prognostic column line model

A 1/3/5-year prognostic line graph was developed utilizing the "rms (6.3.0)" package and visualize the calibration. The sample size of each replicate was 40, and the total number of samples was 200. A 1/3/5-year receiver operating characteristic (ROC) curve analysis of the nomogram was performed using the "timeROC" package.

2.5. Drug sensitivity analysis in the 10-FRDEGs risk scoring model

The drug data of nine OSCC cell lines (Cal27, Cal33, HSC3, HSC2, HSC4, SCC4, SCC9, SCC15, and SCC25) from the Cancer Genome Project were analyzed using the "pRRophetic" package in R. The risk score of each cell line was calculated employing the risk assessment model's risk score formula. The samples' median risk score was used to stratify them into various categories after calculating by risk scoring formula. The differences in effective maximum inhibitory concentration (IC50) values for all drugs between the high- and low-risk groups were determined. Additionally, drugs exhibiting a significant correlation with OSCC sensitivity and risk score were further analyzed (bilateral Pearson correlation test, wherein $p < 0.05$ was considered to indicate a significant correlation). The 3D structures of small-molecule compounds were obtained from the PubChem.

2.6. Single-cell analysis

Single-cell RNA sequencing (scRNA-seq) data from the GSE172577 dataset was analyzed using the "Seurat" package in R. The final selection criteria were 100 < nFeature_RNA <6000 percent.mt < 20, yielding 56686 cells. Following data normalization using the "NormalizeData" function with default parameter settings, highly differentially expressed genes were identified using the "FindVariableFeatures" function and subsequently normalized using the "ScaleData" function for PCA downscaling. Then, the cells were clustered and grouped using the "FindNeighbors" and "FindClusters" functions and visualized using the top 30 principal components for UMAP dimensionality reduction. Following the classification of cells into clusters, we manually identified and annotated the cell clusters using classical marker genes retrieved from the CellMarker database. The "CellCycleScoring" function was used to calculate cell cycle scores and classify OSCC cells. Furthermore, a ferroptosis pathway score was calculated for each single cell using the "AddModuleScore" function in the "Seurat" package in R, deriving scores based on average gene expression levels within the pathway. The resulting scores were used for prognostic modeling of FRDEG expression levels. Ferroptosis pathway scores were calculated as the mean value for each sample across various cell types. A bilateral (two-sided) Pearson correlation test was employed to determine the correlation between the two, with statistical significance denoted by $p < 0.05$.

2.7. Weighted gene co-expression network analysis (WGCNA) and enrichment analysis

The RNA-seq data of OSCC were analyzed using the "Hclust" function in R for hierarchical clustering, with the exclusion of outlier samples. Subsequently, the "pickSoftThreshold" function was used to ascertain an appropriate soft threshold β. We then constructed a hierarchical clustering dendrogram, and genes with similar expressions were classified into distinct modules. Finally, the expression profile of each module was summarized using module eigengenes (ME), and the correlations between the 10-FRDEG risk assessment

model and ME were determined. Using criteria unique to humans, an enrichment analysis of the grey module gene clusters was carried out using the Metascape database.

2.8. qRT-PCR and immunohistochemistry

Four OSCC cell lines (Cal-27, Cal-33, SCC4, and SCC9) and human normal oral keratinocyte epithelial (HOK) cells were purchased from Guangzhou Company. RNA was extracted from OSCC and paraneoplastic tissue, OSCC cell lines, and HOK cells using Trizol (AG RNAex Pro Reagent, China). SYBRGreen (AG, Pro-TaqHS) was used to perform qRT-PCR experiments. The primer sequences used in qRT-PCR can be find in Stable5.The genes names CA9, CAV1, TRIB3, EGFR, and AURKA were entered into the HPA (Human Protein Atlas) database and HNSC with oral tissue action experimental and control groups were selected.

2.9. Cell transfection and in vito functional experiments

SiRNA and transfection reagents were purchased from Guangzhou Reebok Biotechnology Company. CAL-27 and SCC4 cells were transfected according to the instructions.

Cell proliferation of the Cal27 and SCC4 cells was analyzed using a cell counting kit-8 (CCK-8; Tong Ren, Japan). Cell migration of the SCC4 cells was assessed by performing a wound healing assay.The scratch areas were photographed at 0h and 24h, respectively. The Fe^{2+} content in SCC4 cells was measured using Ferroragne (Tong Ren, Japan). The Reactive Oxygen Species (ROS) content in SCC4 cells was measured using ROS assay kit (Bio Sharpe, Chinese). Expression levels of ferroptosis maker genes after transfection with CA9 and CAV1 detected by qpcr.

3. Statistical methods

A statistical analysis was conducted using GraphPad Prism 8 software, and the data were expressed as mean ± standard deviation. Paired t-tests were employed for clinical tissue samples, and two-way comparisons between cell line groups were perform.

4. Results

4.1. Identification and functional analysis of FRDEGs

Differential gene expression analysis was performed using data pertaining to 329 OSCC and 32 paraneoplastic tissues obtained from TCGA database. The essential clinical features of the patients with OSCC are delineated in Table S2. We identified 4671 differentially

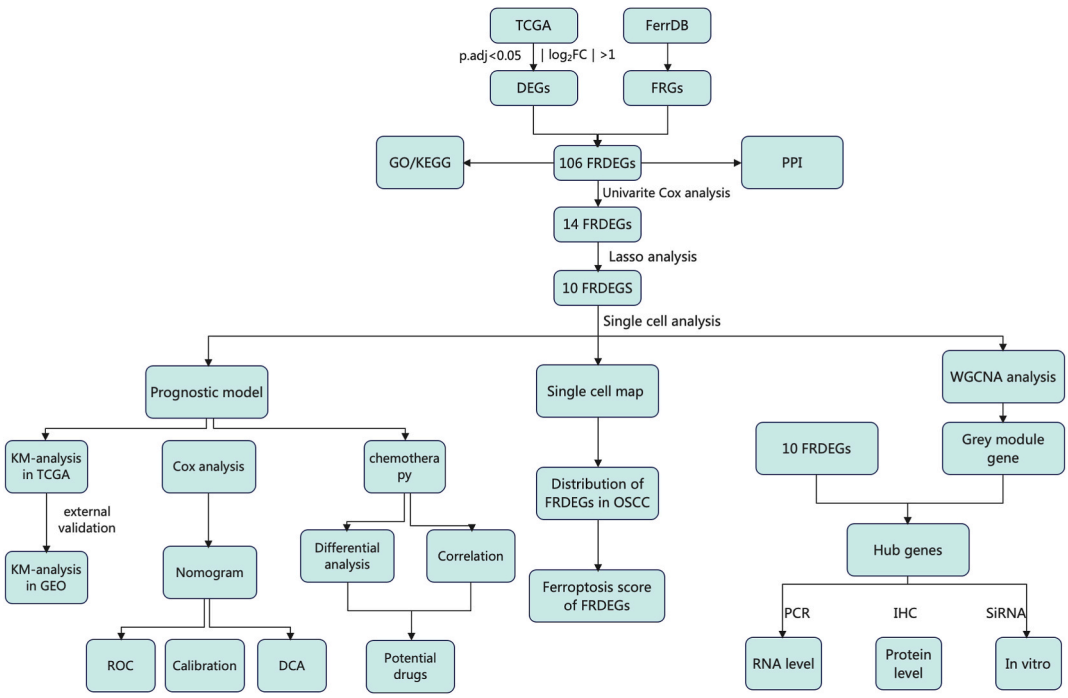

Fig. 1. The flowchart of the research design. The flow chart can be divided into three parts: Dvelopment of a prognostic model; To explore the composition of OSCC at the single-cell level. To explore the potential gene targets of OSCC.

expressed genes and 564 FRGs from the TCGA and FerrDB, respectively(Fig. 2A–B). An intersection between the DEGs in OSCC and FRGs revealed 106 FRDEGs (Fig. 2C). We performed KEGG and GO enrichment analysis on the 106 FRDEGs. GO analysis indicated that FRDEGs were primarily involved in fatty acid metabolism and intracellular redox reactions and the KEGG analysis revealed that FRDEGs were primarily implicated in ferroptosis and the HIF-1 signaling pathway. In addition, Protein-protein interaction (PPI) network shows the interactions between the proteins encoded by the FRDEGs (Fig. S1).

4.2. *Construction of the risk scoring model using the FRDEGs*

To identify FRDEGs strongly linked with the survival status of patients with OSCC, we employed simultaneous univariate Cox analysis on the 106 FRDEGs. The results showed that 14 FRDEGs have potential linked with the survival prognosis of patients with OSCC(Fig. 2D). To mitigate model overfitting, we used LASSO analysis to downscale the FRDEGs. Finally, we identified 10 genes (GOT1, AURKA, EGFR, CAV1, CA9, GRIA3, TRIB3, AKR1C3, TTPA, and PPARG) that exhibited associations with the prognosis of patients with OSCC(Fig. 2E). The risk scoring model was constructed based on the LASSO coefficient and expression of each FRDEG was computed as follows (Figs. 1–4): (0.02499918 × Exp [AURKA]) + (0.09178474 × Exp [TRIB3]) + (0.07867644 × Exp [CAV1]) + (0.09103084 × Exp [CA9]) + (0.34383144 × Exp [GOT1]) + (−0.4916994 × Exp [GRIA3]) + (0.20520292 × Exp [PPARG]) + (−0.914994 × Exp [TTPA]) (Table S2). The risk factor plot of the 10-FRDEG prognostic model illustrated that the median value of the risk scoring model effectively distinguished between the survival outcomes of patients in the low-risk group. Subsequently, the expression of FRDEGs was visualized as a heat map (Fig. 2F).

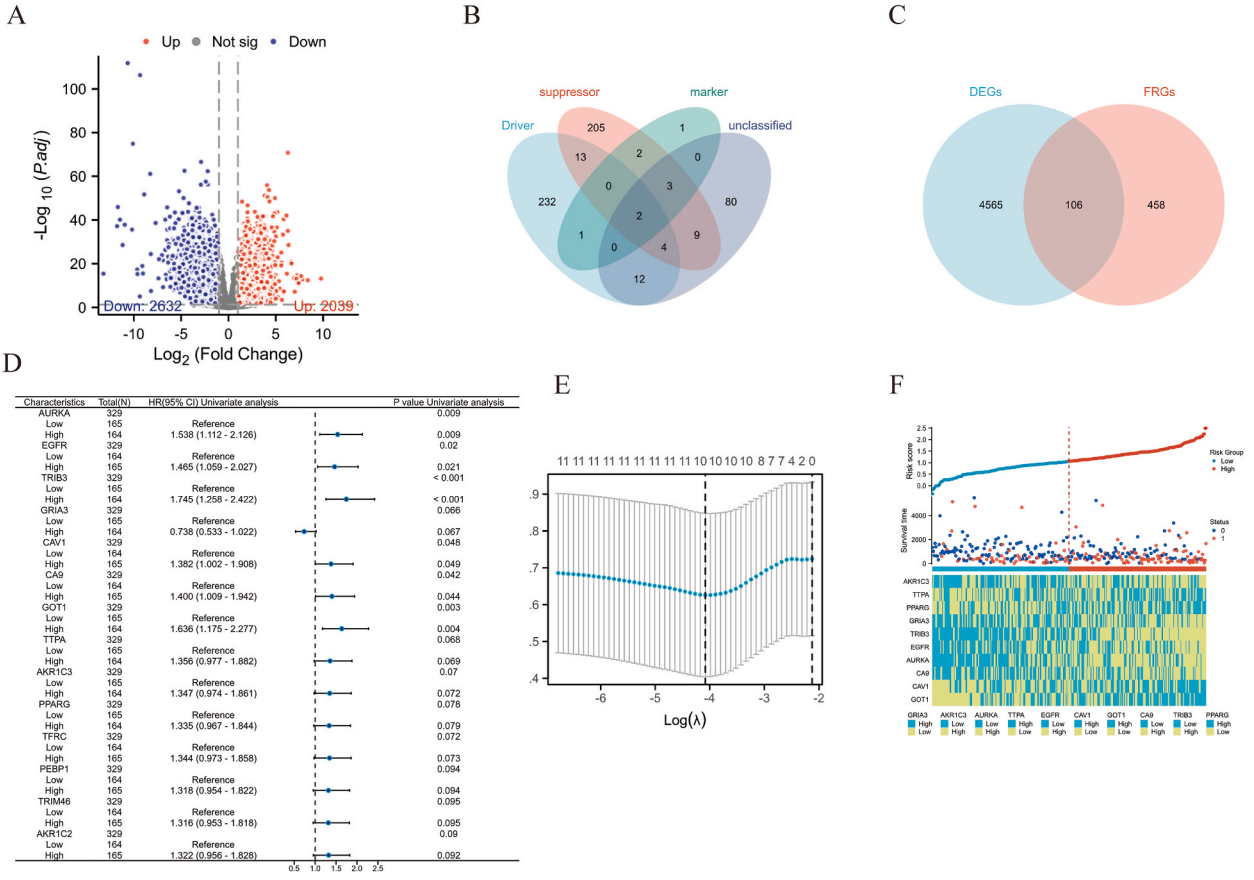

Fig. 2. Construction of 10-FRDEGs risk scoring model in OSCC (A) Differentially expressed genes between OSCC and normal tissue; (B) Screening for ferroptosis-related genes in FerrDb database; (C)The intersection of ferroptosis related genes and differentially expressed genes; (D) The univariate Cox analysis of the 106 FRDEGs; the first *p value* represents the overall variable (category type) in the model, and the second *p value* corresponds to the non-reference group in the variable, excluding the reference group; (E) The lasso regression analysis of the 14 FRDEGs; The lower x-axis denotes the logarithm of penalty term (lambda) values in Lasso regression, while the upper x-axis indicates the count of non-zero coefficients associated with each lambda value. The y-axis represents the c-index across various metrics. A dashed line on the left indicates the lambda value yielding the optimal evaluation metric, whereas a dashed line on the right signifies the lambda value within one standard error range of the optimal value. (F) An analysis of the distribution of risk score, survival time, and heatmaps for 10-FRDEG expression in TCGA.

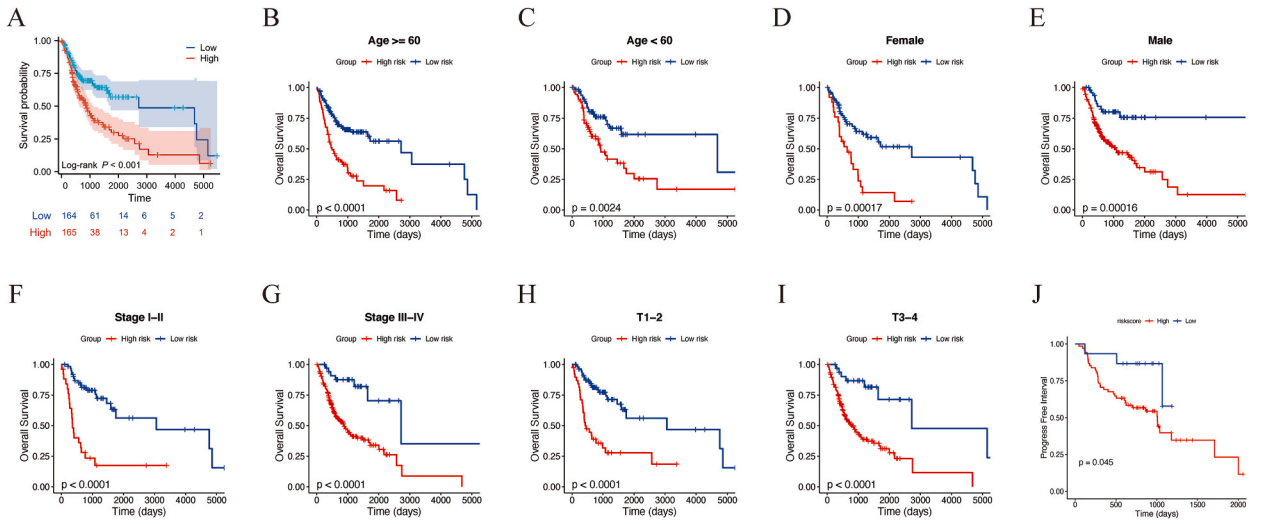

Fig. 3. The survival analysis of 10-FRDEGs risk scoring model in various clinical subtypes in different database. (A) The survival analysis of 10-FRDEGs model in TCGA(A) and in various clinical subtypes and GEO database (B, C, D, E,F,F,G,H,I,J).

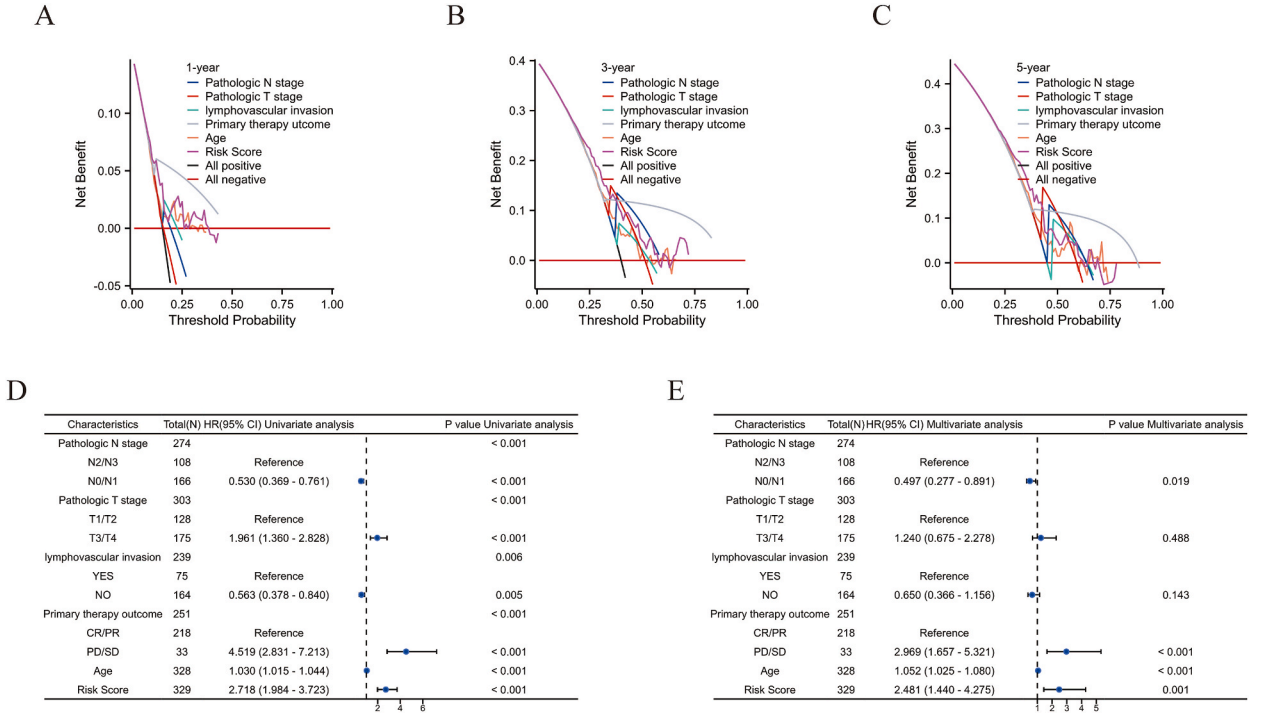

Fig. 4. The validation of 10-FRDEGs risk scoring model. The DCA analysis of 10-FRDEGs risk scoring model in 1 year (A), 3year (B), 5year (C); The Univariate (D) and multivariate cox analysis of 10-FRDEGs risk scoring model.

4.3. Survival analysis using the 10-FRDEGs prognostic model

Survival analysis of patients with OSCC utilizing the 10-FRDEGs model derived from the TCGA database showed that patients in the high-risk group exhibited a significantly worse prognosis compared with others (Fig. 3A). Similarly, survival analysis of the 10-FRDEGs risk scoring model in the GEO database also showed similarly results (Fig. 3J). These results demonstrated that the risk-scoring model had the ability to differentiate the prognosis of a cohort of patients with OSCC in the various dataset.

In addition to conducting the survival analysis of overall OSCC patients in the TCGA database, an analysis of various clinical subtypes of patients with OSCC were performed using the risk scoring model. Survival analysis was performed for patients in the OSCC

clinical subgroups showed that patients in the high-risk category had significantly worse OS rates (Fig. 3B–I). These results demonstrated the robust predictive capacity of the risk-scoring model across stratified clinical subgroups of patients with OSCC.

4.4. Validation of the risk scoring model for 10-FRDEGs

To assess the clinical utility of the 10-FRDEGs risk scoring model, we conducted a 1/3/5-year DCA curve analysis of the 10-FRDEGs risk scoring model. The DCA cruve showed that across a defined threshold range, the 10-FRDEG prognostic model's 1/3/5-year DCA curves consistently exhibited greater significance compared to other clinicopathological features, whether considering all positive or all negative outcomes, thereby demonstrating the superior clinical value offered by the 10-FRDEG model. (Fig. 4A–C). To further explore the independence of the model in predicting OSCC prognosis status, we employed simultaneous univariate and multivariate Cox analyses of the 10-FRDEGs risk scoring model using clinicopathological characteristic data of patients with OSCC. Univariate Cox analysis founded that pathologic N stage, pathologic T stage, lymphovascular invasion, primary therapy outcome, age, and the 10-FRDEGs risk scoring model were all significant factors influencing the prognosis (Fig. 4D, $p < 0.1$). Multivariate Cox analysis indicated that pathological N stage, primary therapy outcome, age, and the 10-FRDEGs risk scoring model were significantly linked with the prognosis and could be employed as independent prognostic indicators (Fig. 4E, $p < 0.05$).

4.5. Prognostic column line graph construction and validation

To predict the survival outcomes of individual patients with OSCC accurately, we developed a 1/3/5-year prognostic column line graph (Nomogram). To this end, we employed the clinicopathological characteristics that were strongly linked with the prognosis of individual with OSCC and the 10-FRDEGs risk scoring model as variables (Fig. 5A). To verify the prediction accuracy of the nomogram for 1/3/5-year survival rates., calibration curves were created. The results revealed that the nomogram exhibited a high degree of overlap between the 1/3/5-year prediction line and the ideal line, thereby demonstrating that the established model exhibited a high degree of similarity to the ideal model (Fig. 5B–D).

Furthermore, we performed ROC analysis of the nomogram column plots to determine the accuracy of its prediction results. The findings demonstrated the excellent reliability of the model's 1/3/5-year predictions, with the area under the time-dependent ROC curve (AUC) of the nomogram for 1/3/5 years being 0.791, 0.798, and 0.716, respectively (Fig. 5E–G). Finally, we also evaluated the

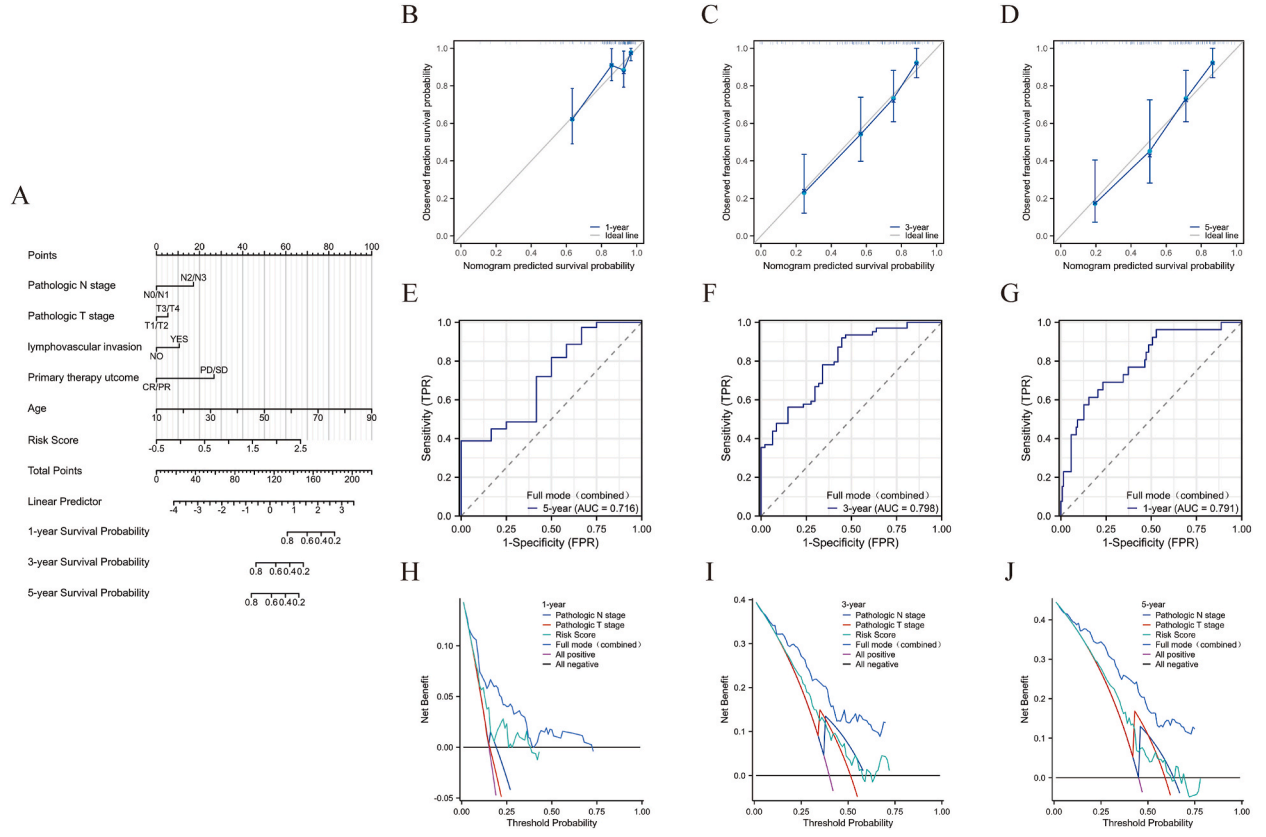

Fig. 5. Construction and validation of a nomogram. (A) Nomogram model to predict 1-, 3-, or 5-year survival in OSCC patients. The 1 (B),3(C),5(D) year calibration curve of nomogram. The 1 (E),3(F),5(G)year ROC curve of nomogram. The 1 (H),3(I),5(J)year DCA curve of nomogram.

clinical value of various variables including the 10-FRDEGs risk scoring model. The results of the DCA curves for 1/3/5-year showed that the clinical utility of the nomogram was consistently superior to others (Fig. 5H–J). Therefore, the nomogram exhibits superior predictive reliability compared to other predictors, potentially enhancing the precision of the prognosis for patients with OSCC in clinical practice.

4.6. I identification of potential chemotherapeutic drugs for patients with OSCC

To further explore personalized therapeutic interventions for patients with OSCC in clinical settings, we analyzed the IC50 values to estimate the responsiveness of patients with OSCC to chemotherapy. The results founded that the different risk subgroups of the 10-FRDEGs risk scoring model exhibited varying sensitivity to the primary small molecule compounds. The OSCC cell in the low-risk category exhibited more sensitivity to (5Z)-7-oxozeaenol, KIN00-266, and AT-7519, whereas OSCC cells in the high-risk category exhibited more sensitivity to PF-562271 and LFM-A13 (Fig. 6A–E). Concurrently, we conducted the correlation analysis between drug susceptibility and risk of various small molecule compounds in OSCC. The results revealed a strongly correlation between the drug susceptibility of various small molecules and the risk score of patients with OSCC (Fig. 6F–J).

Finally, through the intersection of the results derived from further analysis with those obtained from the correlation analysis, we identified (5Z)-7-oxozeaenol, AT-7519, and KIN001-266 (Figs. 1–5-A) and further investigated their respective 3D structures (Fig. S2). Thus, (5Z)-7-oxozeaenol, AT-7519, and KIN001-266 exhibit potential as chemotherapeutic agents for OSCC cell in the low-risk category of the 10-FRDEGs risk scoring model. This finding provides a promising avenue for the development of targeted OSCC cell chemotherapy.

4.7. Distribution and functional status of FRDEGs in the OSCC microenvironment

To investigate the distribution of FRDEGs in the OSCC microenvironment, we analyzed single-cell data of OSCC. To this end, the single-cell data of OSCC were downscaled, and the cells were clustered and sub-clustered. Subsequently, OSCC cells were classified into nine distinct cell types, namely epithelial, myocyte, fibroblast, endothelial, myeloid, B, T, plasma, and mast cells. To further validate the accuracy of the single-cell clusters based on cell type, we examined the expression levels of marker genes associated with each defined cell type. The results showed that the expression pattern of marker genes was consistent across cell types, demonstrating that the cells were accurately classified into single-cell clusters. In addition to categorizing OSCC cells based on cell type, OSCC tissues were differentiated based on cell cycle at the single-cell level. The results showed that the majority of OSCC cells were in the G1, G2, M, and S phases. To further refine the statistics on the number and relative content of various cell types in OSCC, we analyzed the proportion of different cell types in OSCC(Figs. S3A–E).

Furthermore, we analyzed the expression levels of the FRDEGs in each of the nine cell types of OSCC(Fig. 7). The figure revealed that the FRDEGs were enriched in the epithelial cells of OSCC, thereby demonstrating their predominant activity through epithelial cells in OSCC. In addition, to investigate the relationship between the FRDEGs and proliferative divisions of OSCC in the constructed

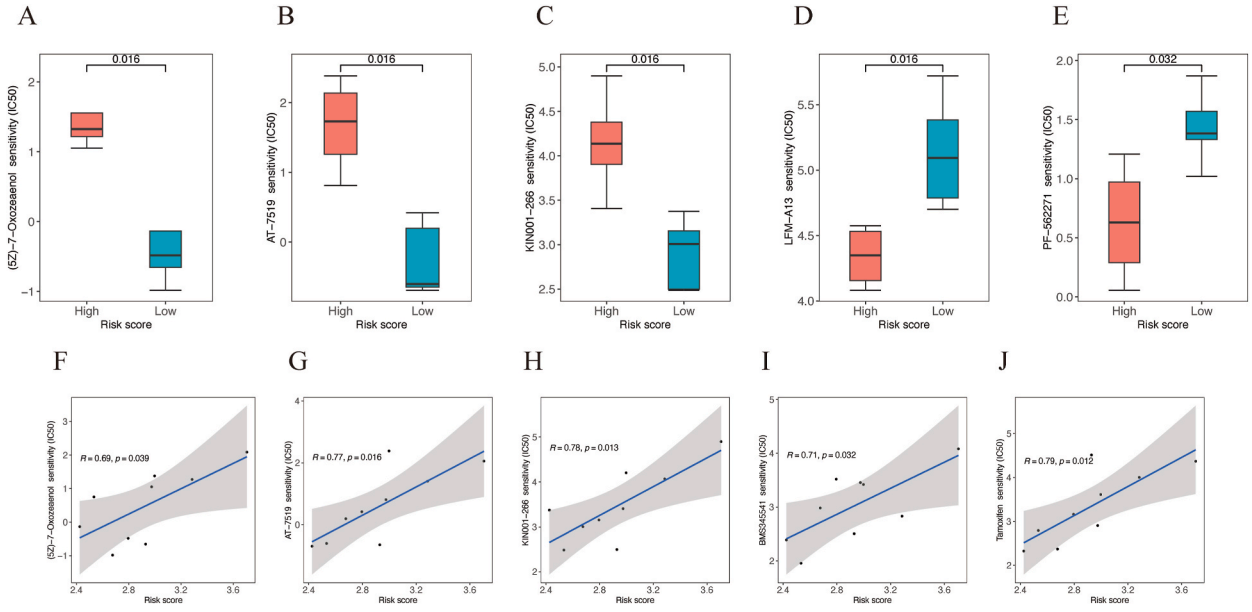

Fig. 6. The potential drugs for the chemotherapy of patients with OSCC. The sensitivity of 5Z)-7-oxozeaenol(A), AT-7519(B), KIN00-266(C), LFM-A13(D) and PF-562271(E) in high and low risk categories. The correlation of 5Z)-7-oxozeaenol(F), AT-7519(G), KIN00-266(H), BMS345541(I), tamoxifen(J) sensitivities with the risk scores of 10-FRDEGs model.

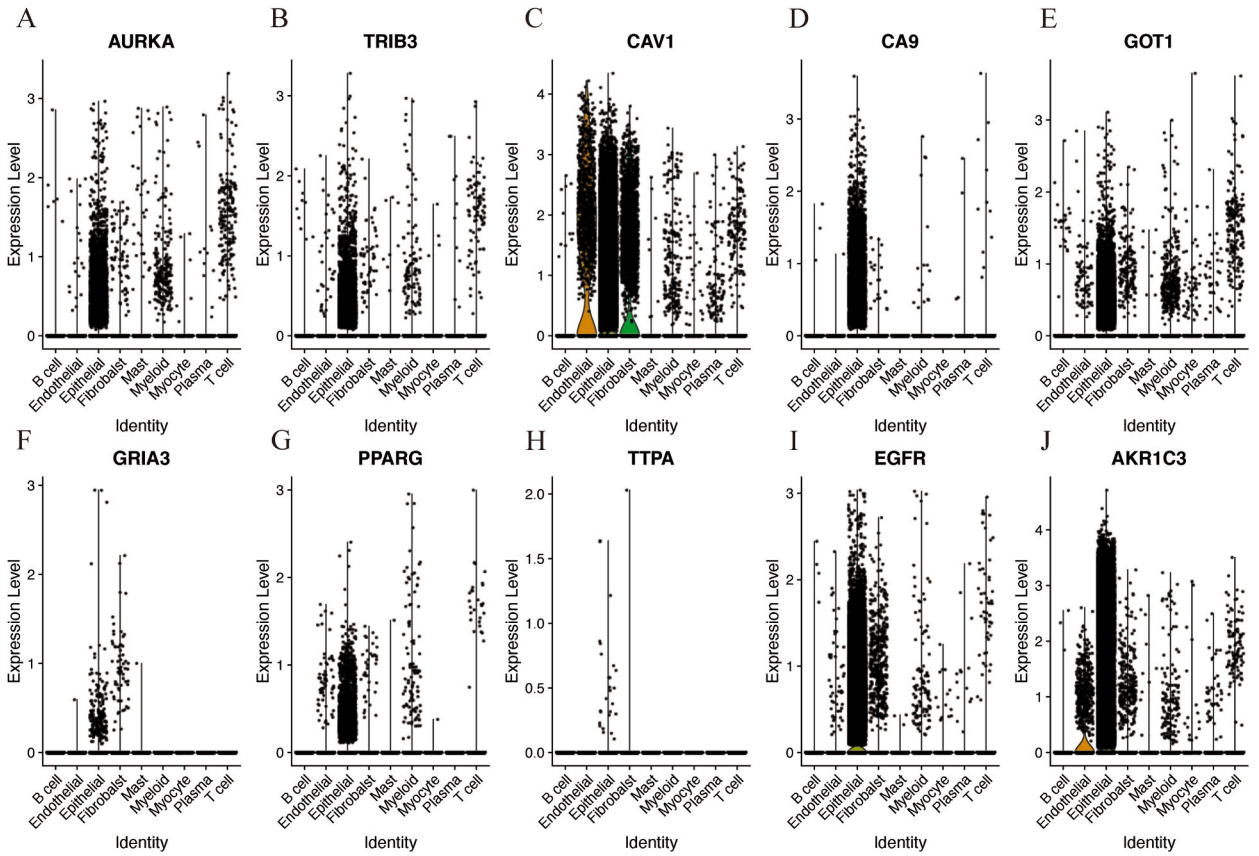

Fig. 7. The distribution of FRDEGs in the OSCC microenvironment.

OSCC prognostic model, we investigated their expression levels during various cell cycle phases (Fig. S3F).

To assess the correlation between the 10-FRDEGs model and ferroptosis status, we first performed a series of correlation analyses between nine cell types and ferroptosis scores. We found that in OSCC, epithelial cells showed the highest correlation with ferroptosis. To further explore the relationship among the FRDEGs, which constituted the foundation of the risk assessment model, and ferroptosis in OSCC, we analyzed the correlations between FRDEGs across various cell types and ferroptosis scores. The results showed that the *AKR1C3* and *CA9* genes were more closely associated with ferroptosis in OSCC epithelial cells. Additionally, *TRIB3*, *EGFR*, and *GOT1* were found to be closely associated with ferroptosis in T cells(Fig. S4).

4.8. Identification of the mechanism and hub genes of 10-FRDEGs model

To identify the gene modules associated with the risk scoring model constructed using the 10 FRDEGs, RNA-seq data from OSCC patients in the TCGA were extracted for WGCNA. Highly covariant sets of module genes were identified, and their expression characteristics were summarized. Scale-free topology analysis showed that the appropriate soft threshold β was 4 (achieving scale independence) for this analysis. Mean connectivity analysis was subsequently performed to determine the average connectivity value stabilized at a soft threshold of 4(Fig. 8A–B). Subsequently, co-expressed gene modules were constructed and divided into multiple meaningful modules (Fig. 8C). By analyzing the association between the various gene modules and the 10-FRDEGs risk scoring model, we determined that nine gene modules were each associated with the 10-FRDEGs model (Fig. 8D). Notably, the grey module exhibited the most significant contribution to the 10-FRDEGs risk scoring model.

Further enrichment analysis of the grey module gene module revealed that several biological processes, including epidermal development (GO:0008544), neutrophil degranulation (R-HSA-6798695), photomorphogenesis (GO:0048729), and signaling by interleukins, as the most important biological processes affecting the risk score of patients with OSCC (Fig. 8E). To identify the hub genes in the 10-FRDEGs model, we intersected the grey module gene module with the 10-FRDEGs, ultimately identifying four hub genes, namely CA9, CAV1, AURKA, and EGFR (Fig. 8F).

4.9. Validation of the expression level of FRDEGs

We initially examined the RNA expression levels of the FRDEGs in the OSCC clinical samples compared to normal tissues

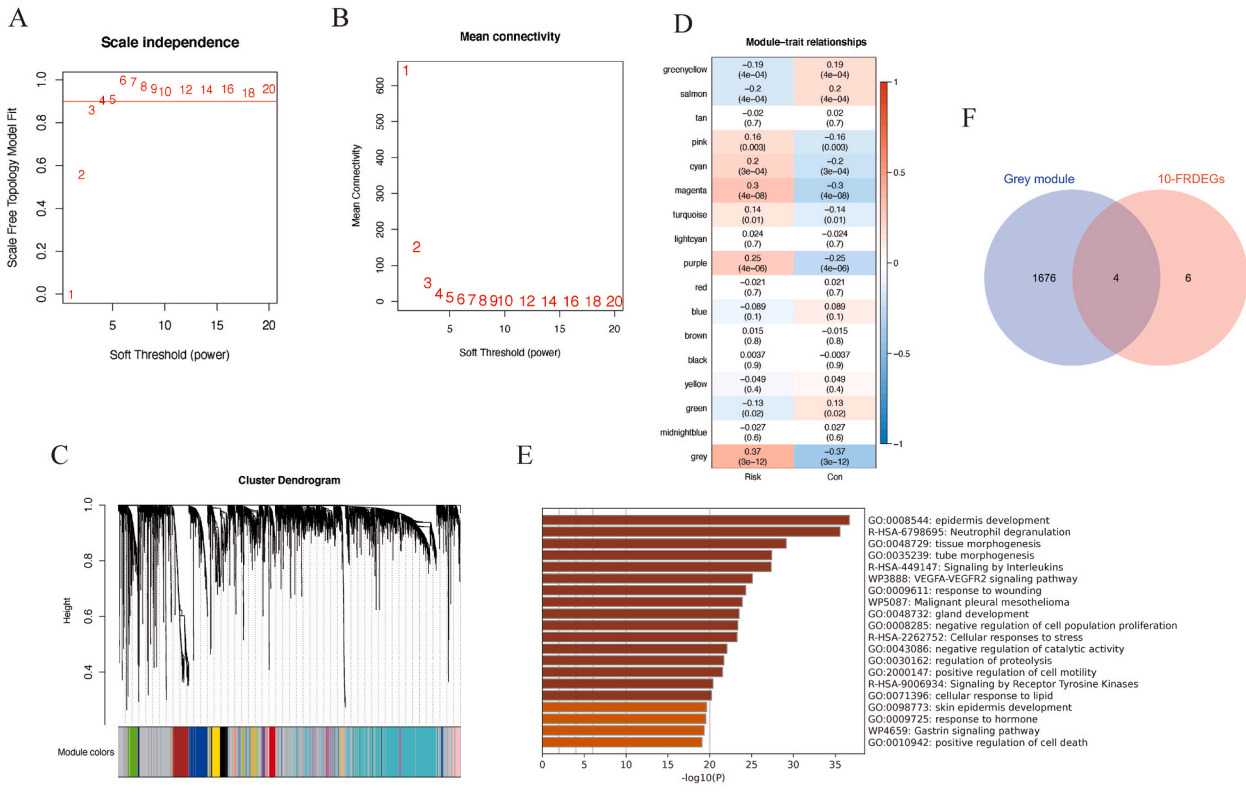

Fig. 8. The WGCNA analysis and identification of hub genes. (A–B) Examining and verifying of the soft threshold; (C) Clustering dendrogram of genes in OSCC; (D) Correlation between various gene modules and risk scoring model; (E) Enrichment analysis of grey gene module; (F)Identification of the hub genes in grey gene module.

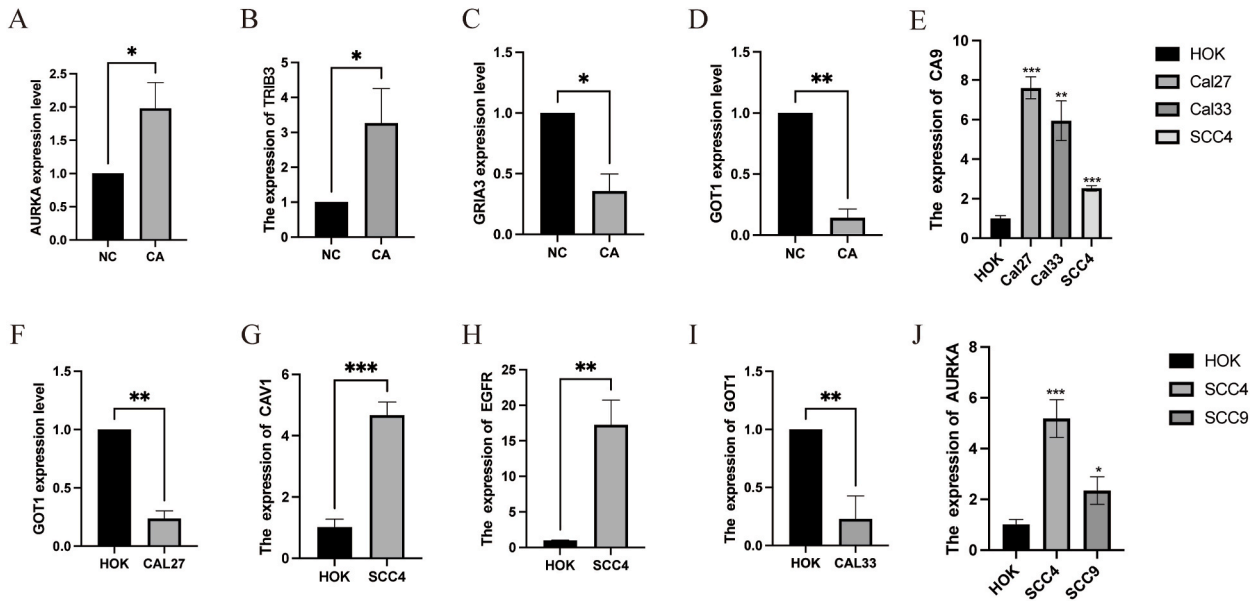

Fig. 9. The RNA expression level of FRDEGs between OSCC and Normal tissue. *Present $p < 0.05$, ** present $p < 0.01$, *** present $p < 0.001$.

(Fig. 9A–D). In OSCC, AURKA, TRIB3, CA9, and CAV1 were markedly overexpressed, while GOT1 and GRIA3 were downregulated. Subsequently, RNA expression levels of the FRDEGs were further validated across various cell lines (Fig. 9E–J). The results revealed that CA9, CAV1, EGFR, and AURKA were markedly overexpressed in OSCC cell lines, whereas GOT1 was markedly downregulated in

OSCC. Finally, immunohistochemistry was performed to analyze the protein expression levels of the FRDEGS in OSCC tissue microarrays compared to normal oral tissues (Fig. 10). The results showed that AURKA, TRIB3, CA9, CAV1, and EGFR were markedly overexpressed in OSCC.

4.10. CA9 and CAV1 regulate the malignance of OSCC

CA9 and CAV1, which were the hub genes of OSCC that are yet to be studied, were further analyzed for their functions and roles in OSCC. SiRNA was employed to knockdown CA9 and CAV1 in Cal27 and SCC4 cells, respectively. Subsequently, qRT-PCR analysis demonstrated that the knockdown of CA9 and CAV1 is successful (Fig. S4). Furthermore, CCK-8 assays demonstrated that the knockdown of CA9 and CAV1 expression in Cal27 and SCC4 cells resulted in a markedly inhibit in the cell proliferative capacity (Fig. 11A–B). The wound healing assay showed a significant decrease in the migratory ability of SCC4 cells after the knockdown of CA9 and CAV1 expression (Fig. 11C). The Fe^{2+} assay showed a significant increase in intracellular Fe^{2+} levels in both Cal27 and SCC4 cells post-CA9 and CAV1 knockdown, which conversely decreased upon the addition of the ferroptosis inhibitor Fer-1(Fig. 11D). The lipid peroxide assay showed that the intracellular levels of lipid peroxide in both Cal27 and SCC4 cells increased significantly following the knockdown of CA9 and CAV1, which were mitigated upon the addition of Fer-1(Fig. 11E). Finally, qRT-PCR showed that the expression of ferroptosis marker genes was significant decreased after knockdown of CA9 and CAV1 (Fig. 11F–G). These results demonstrated that the knockdown of CA9 and CAV1 resulted in the inhibition of proliferation and migration of OSCC cells while promoting ferroptosis.

5. Discussion

The prognosis of patients with tumors is often a critical clinical concern for both medical practitioners and patients. Therefore, there exists an urgent clinical need for a novel approach to tumor cell biology that can aid in the improvement of the accuracy of the prognosis of patients with tumors. Ferroptosis occurs primarily result from cell membrane rupture and death caused by intracellular iron ion-dependent accumulation of lipid peroxides [20]. Recently, FRGs were identified as prognostic markers for various tumors (e.

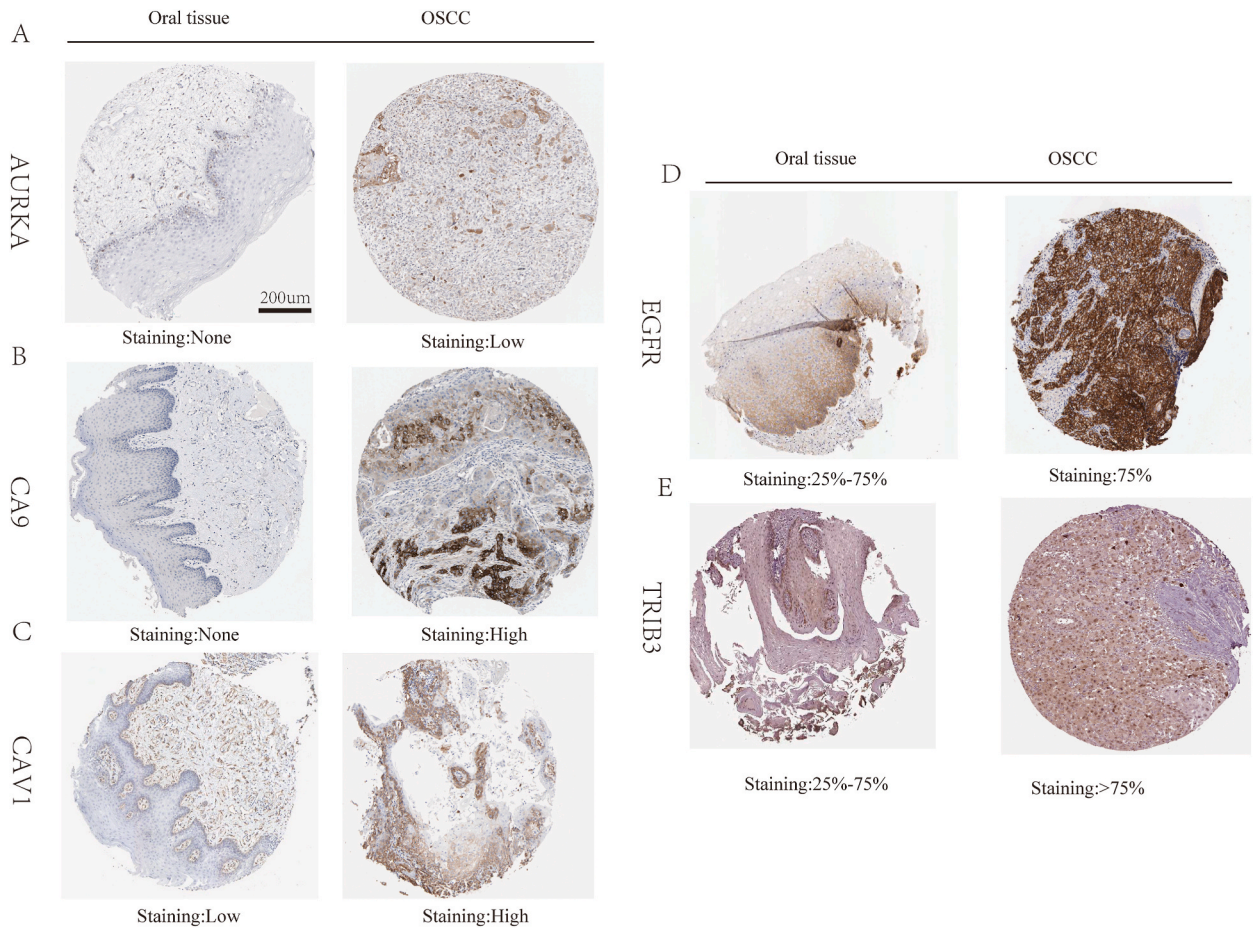

Fig. 10. The protein expression level of FRDEGs between OSCC and Normal tissue.

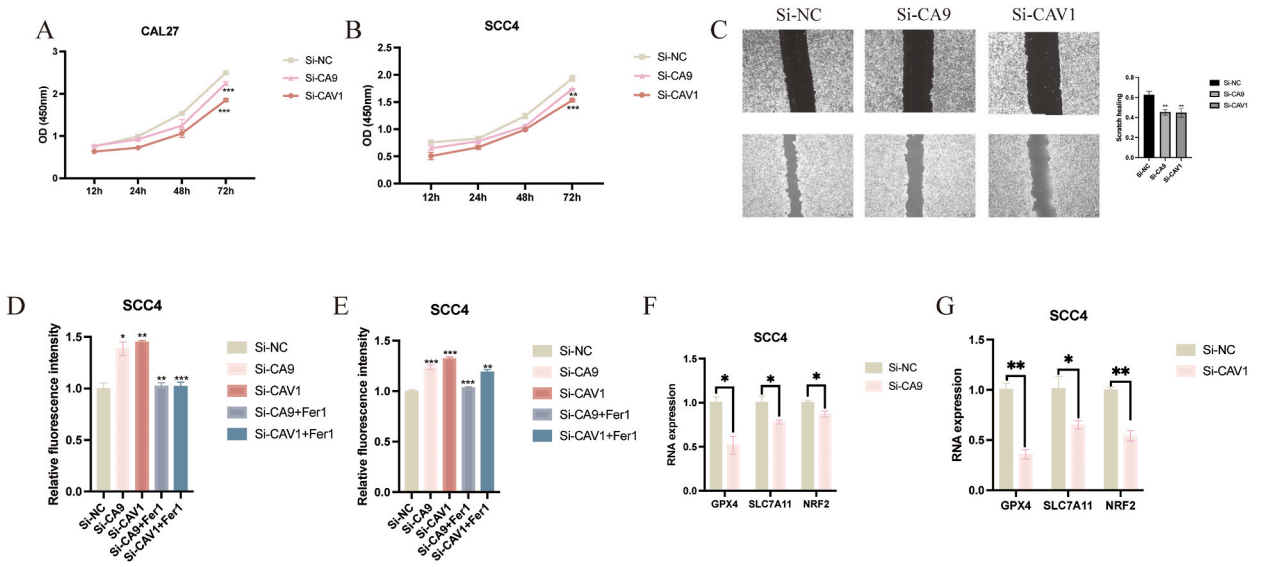

Fig. 11. The functional validation of the CA9 and CAV1 in OSCC cell line. The proliferative effect of CA9 and CAV1 on Cal27(A) and SCC4 (B) evaluated by CCK8 tests; (C)The migration effect of CA9 and CAV1 on SCC4 evaluated by wound healing experiment; (D) The regulate effect of CA9 and CAV1 on the levels of intracellular $Fe2^{+}$ in SCC4. (E)The regulate effect of CA9 and CAV1 on the levels of intracellular ROS in SCC4. (F–G) The regulate effect of CA9 and CAV1 on the levels of ferroptosis related genes in SCC4. *Present $p < 0.05$, ** present $p < 0.01$, *** present $p < 0.001$.

g., liver cancer, osteosarcoma, glioma, and colon cancer) [21–24]. In addition, a few genes have been found to exert additional influence on tumor progression by regulating the ferroptosis mechanism in OSCC [25]. Given the intimate association between ferroptosis and the progression and prognosis of numerous tumors, including OSCC, we leveraged ferroptosis genes to develop a prognostic model to tailored to OSCC and identify potential chemotherapeutic agents and molecular targets for the treatment of patients with OSCC.

In this study, we employed bioinformatics to identify10 FRDEGs associated with survival status of patients with OSCC and constructed a risk scoring model. FRDEGs have been found to be closely associated with various other cancers, and the regulation of OSCC. Shen et al. elucidated that TRIB3 promotes the progression of OSCC by activating the AKT signaling pathway [26]. Another study showed that AURKA regulates apoptosis and epithelial-mesenchymal transition in OSCC by mediating the production of ROS [27]. Zhang et al. elucidated that EGFR regulates the sensitivity of OSCC cells to JQ1 (an antitumor agent) through a signaling pathway [28]. In addition, another study showed that EGFR modulates the malignant mechanisms of OSCC by regulating sequestosome-1, an autophagy-related protein [29].

Survival and DCA analysis of the ferroptosis prognostic model revealed that the prognostic model significantly differentiated the survival of patients in different risk categories, thereby exhibiting notable clinical benefits. Furthermore, a nomogram was developed by combining the ferroptosis prognostic model with other clinicopathological features to predict the 1/3/5 more accurately-year survival probability of patients with OSCC. Calibration curve analysis, ROC analysis, and DCA of the nomogram column plots showed that the nomogram exhibited high reliability and that the nomogram column plots can be used to determine the likelihood of a clinical event by assigning scores to various observations and calculating the total score [30,31]. In contrast to TNM staging, the nomogram is based on a multivariate cox analysis to establish a scoring scale that characterizes the variables in the multivariate regression model. The total score is calculated to assess the probability of an event. DCA is used to evaluate clinical prediction models and biomarkers [32]. DCA curves are different from ROC curves in terms of validating the model, with the former considering the clinical utility of the model and the latter considering the model's accuracy in terms of sensitivity and specificity.

By performing differential drug sensitivity analysis and correlation analysis, we finally identified three small molecule compounds specific to patients with OSCC in the high-risk category, namely (5Z)-7-oxozeaenol, AT-7519, and KIN001-266. 5Z)-7-Oxozeaenol, an inhibitor of the NF-κB pathway, can improve sensitivity to ROS-induced apoptosis and adhesion in breast cancer cells [33]. Due to the NF-κB pathway can promote the progression of OSCC, (5Z)-7-oxozeaenol as an inhibitor of the NF-κB pathway is a potential therapeutic drug for OSCC [34]. A study showed that AT-7519 (a cyclin-dependent kinase) is a cell cycle-dependent kinase inhibitor with the potential to mitigate multi-drug resistance through in vitro assays [35].Furthermore, OSCC development and incidence are linked to cyclin-dependent kinases (CDK4 and CDK6). Therefore, AT-7519 may have inhibitory effects on OSCC [36]. In addition, MAP3K8 overexpression is linked to OSCC development in murine salivary glands. Therefore, KIN001-266, as an inhibitor of MAP3K8, has potential inhibitory effects on OSCC [37].To date, no studies have explored the effects of 5Z)-7-Oxozeaenol, AT-7519, and KIN001-266 on OSCC. Therefore, this study provides novel insights and avenues for further investigation into patient-specific chemotherapy regimens for the treatment of OSCC.

OSCC is an integral group of malignant, immune, and stromal cells that exhibit marked intra-tumoral and inter-tumoral heterogeneity. Therefore, a comprehensive and segmented analysis of cellular, functional, and genetic characteristics of OSCC at single-cell

level is required [38]. A recently created method called ScRNA-seq enables the non-targeted measurement of transcripts at the level of individual cells in tissues. Many studies have reported the extensive applicability of ScRNA-seq for the investigation of cancers, including HNSC, breast cancer, and so on [39–41].Moreover, to better investigate the distribution and functional status of FRDEGs within the OSCC microenvironment, we constructed a single-cell atlas of OSCC using an OSCC single-cell dataset. The single-cell atlas showed that OSCC cells are highly proliferative and that epithelial cells are the primary malignant cells in OSCC. We then investigated the expression of 10 FRDEGs across various cell types and cycles of OSCC. The results indicated that the majority of FRDEGs were primarily expressed in epithelial and G1-phase cells. These results demonstrate that FRDEGs act in OSCC mainly by affecting epithelial cells. Additionally, a detailed investigation of the ferroptosis scores of the various cell types and FRDEGs in OSCC at single cell level was performed. The results showed that epithelial and G1-phase cells were most closely associated with ferroptosis in OSCC. At the same time, AKR1C3, GOT1, EGFR, PPARG, CA9, and TRIB3 were also discovered to be substantially correlated with ferroptosis in various cell types.

Finally, to elucidate the molecular mechanisms driving the 10-FRDEGs model, we performed WGCNA and screened the key module gene clusters most associated with the 10-FRDEGs risk scoring model. Furthermore, we performed an enrichment analysis to identify the biological processes that played the most critical role in risk scoring. WGCNA revealed that the grey module gene cluster was the most relevant to the risk scoring of the 10-FRDEGs model. Enrichment analysis of the grey module gene cluster revealed that epidermal development (GO:0008544), neutrophil degranulation (R-HSA-6798695), histomorphogenesis (GO:0048729), and signaling by interleukins, were the primary biological processes that influenced the 10-FRDEGs model.

The development of molecularly targeted therapies for tumors has experienced rapid progress in recent years, leading to a notable improvement in the therapeutic efficacy of many tumors [42–44]. However, advancements in molecularly targeted therapies for OSCC continue to fall behind compared to those for other types of tumors. Therefore, developing molecularly targeted therapies for OSCC is imperative. CA9, CAV1, AURKA, and EGFR are the hub genes of the 10-FRDEGs model and are markers and molecular targets of poor prognosis in patients with OSCC. So far, some progress has been achieved in the investigation of the regulatory roles of AURKA and EGFR in OSCC [27,29].However, CA9 and CAV1 are only linked with the susceptibility and prognosis of patients with OSCC [45,46]. In this study, to identify novel molecular therapeutic targets for OSCC based on the 10-FRDEGs risk scoring model in OSCC, we investigated the RNA and protein expression levels and molecular functions of CA9 and CAV1. The results indicated that CA9 and CAV1 are aberrantly expressed in OSCC. In vitro functional assays performed after knocking down the expression of CA9 and CAV1 using si-RNA revealed that CA9 and CAV1 play a role in various malignant behavior, such as proliferation, migration, and ferroptosis, in OSCC cells. Therefore, our study is the first to investigate CA9 and CAV1 as therapeutic targets for OSCC and provides novel avenues and insights for the development of molecularly targeted therapies for OSCC.

There are certain restrictions on our study, though. First, the prognostic assessment model of ferroptosis could not be validated using clinical data. Second, the regulatory role of CA9 and CAV1 on the malignant behavior of OSCC could not be validated through in vivo tests. Finally, the mechanisms by which CA9 and CAV1 regulate malignant behavior in OSCC could not be elucidated.

6. Conclusions

In this research, we employed bioinformatics to construct a novel 10-FRDEG risk scoring model for OSCC, offering enhanced prognostic capabilities for patients with OSCC. In addition, based on the 10-FRDEG risk assessment model, three therapeutic small molecules were identified for OSCC cell in the low-risk group. Furthermore, the present study revealed that FRDEGs are primarily enriched in epithelial cells in the OSCC microenvironment and are closely associated with ferroptosis from single-cell level. This study has finally shown that CA9 and CAV1 are hub genes in the risk score model and may be potential molecular treatment targets for OSCC. This was previously not known.

Ethics statement

OSCC tissues and paraneoplastic tissues were obtained from the Southern Medical University Stomatology Hospital. All patients signed an informed consent form, and this study was approved by the ethical review committee of Southern Medical University.The ethics approval number is EC-CT-[2022]21.

Funding

This research was funded by the Science and Technology Project of Guangzhou City (201802020018) and the Guangdong Science and Technology Program (2019A1515010408).Open access funding provided by Stomatological Hospital, School of Stomatology, Southern medical univeristy.

Institutional review board statement

The Ethics Committee of Southern Medical University's Stomatological Hospital granted ethics permission prior to participation in the research, all patients provided written informed consent.

Informed consent statement

The patients have provided written, informed consent for the publication of this information.

Data availability statement

Original contributions described in the research may be found in the article/Supplementary Material. Contact the appropriate authors with any more questions.

CRediT authorship contribution statement

Zhengming Tang: Writing – original draft, Formal analysis, Conceptualization. **Yuanxin Chen:** Software. **Yisheng Huang:** Software. **JianJiang Zhao:** Writing – original draft. **Bo Jia:** Writing – review & editing, Conceptualization.

Declaration of competing interest

The authors declare that they have no known competing financial interests or personal relationships that could have appeared to influence the work reported in this paper.

Acknowledgments

No.

Appendix A. Supplementary data

Supplementary data to this article can be found online at https://doi.org/10.1016/j.heliyon.2024.e31676.

References

[1] J. Ali, et al., Genetic etiology of oral cancer, Oral Oncol. 70 (2017) 23–28.
[2] S. Sahar, P. Sassone-Corsi, Metabolism and cancer: the circadian clock connection, Nat. Rev. Cancer 9 (12) (2009) 886–896.
[3] F. Bray, et al., Global cancer statistics 2018: GLOBOCAN estimates of incidence and mortality worldwide for 36 cancers in 185 countries, CA Cancer J Clin 68 (6) (2018) 394–424.
[4] M. Mascitti, et al., An overview on current non-invasive diagnostic devices in oral oncology, Front. Physiol. 9 (2018) 1510.
[5] R.L. Siegel, et al., Cancer statistics, 2021, CA Cancer J Clin 71 (1) (2021) 7–33.
[6] M. Gospodarowicz, et al., History and international developments in cancer staging, Cancer Prev Control 2 (6) (1998) 262–268.
[7] M.B. Amin, et al., The Eighth Edition AJCC Cancer Staging Manual: continuing to build a bridge from a population-based to a more "personalized" approach to cancer staging, CA Cancer J Clin 67 (2) (2017) 93–99.
[8] S. Blatt, et al., Biomarkers in diagnosis and therapy of oral squamous cell carcinoma: a review of the literature, J. Cranio-Maxillo-Fac. Surg. 45 (5) (2017) 722–730.
[9] H. Li, et al., Ferroptosis-related gene signature predicts the prognosis in Oral squamous cell carcinoma patients, BMC Cancer 21 (1) (2021) 835.
[10] S.J. Dixon, et al., Ferroptosis: an iron-dependent form of nonapoptotic cell death, Cell 149 (5) (2012) 1060–1072.
[11] H.F. Yan, et al., Ferroptosis: mechanisms and links with diseases, Signal Transduct Target Ther 6 (1) (2021) 49.
[12] X. Jiang, B.R. Stockwell, M. Conrad, Ferroptosis: mechanisms, biology and role in disease, Nat. Rev. Mol. Cell Biol. 22 (4) (2021) 266–282.
[13] Z. Tang, et al., Ferroptosis: the silver lining of cancer therapy, Front. Cell Dev. Biol. 9 (2021) 765859.
[14] H.T. Wang, et al., Insights into ferroptosis, a novel target for the therapy of cancer, Front. Oncol. 12 (2022) 812534.
[15] R. Tang, et al., Ferroptosis, necroptosis, and pyroptosis in anticancer immunity, J. Hematol. Oncol. 13 (1) (2020) 110.
[16] L. Zhao, et al., Ferroptosis in cancer and cancer immunotherapy, Cancer Commun. 42 (2) (2022) 88–116.
[17] Y. Su, et al., Ferroptosis, a novel pharmacological mechanism of anti-cancer drugs, Cancer Lett. 483 (2020) 127–136.
[18] Y. Wang, et al., The function and mechanism of ferroptosis in cancer, Apoptosis 25 (11–12) (2020) 786–798.
[19] Y. Yang, et al., The PER1/HIF-1alpha negative feedback loop promotes ferroptosis and inhibits tumor progression in oral squamous cell carcinoma, Transl Oncol 18 (2022) 101360.
[20] Y. Wu, et al., The epigenetic regulators and metabolic changes in ferroptosis-associated cancer progression, Mol. Cancer 19 (1) (2020) 39.
[21] Z. Xu, et al., Construction of a ferroptosis-related nine-lncRNA signature for predicting prognosis and immune response in hepatocellular carcinoma, Front. Immunol. 12 (2021) 719175.
[22] R.J. Wan, et al., Ferroptosis-related gene signature predicts prognosis and immunotherapy in glioma, CNS Neurosci. Ther. 27 (8) (2021) 973–986.
[23] T. Lei, et al., Ferroptosis-related gene signature associates with immunity and predicts prognosis accurately in patients with osteosarcoma, Cancer Sci. 112 (11) (2021) 4785–4798.
[24] H.J. Cai, et al., Development and validation of a ferroptosis-related lncRNAs prognosis signature in colon cancer, Bosn. J. Basic Med. Sci. 21 (5) (2021) 569–576.
[25] K. Sun, et al., MiR-34c-3p upregulates erastin-induced ferroptosis to inhibit proliferation in oral squamous cell carcinomas by targeting SLC7A11, Pathol. Res. Pract. 231 (2022) 153778.
[26] P. Shen, T.Y. Zhang, S.Y. Wang, TRIB3 promotes oral squamous cell carcinoma cell proliferation by activating the AKT signaling pathway, Exp. Ther. Med. 21 (4) (2021) 313.
[27] H. Dawei, D. Honggang, W. Qian, AURKA contributes to the progression of oral squamous cell carcinoma (OSCC) through modulating epithelial-to-mesenchymal transition (EMT) and apoptosis via the regulation of ROS, Biochem. Biophys. Res. Commun. 507 (1–4) (2018) 83–90.
[28] X. Liu, et al., EGFR-mediated signaling pathway influences the sensitivity of oral squamous cell carcinoma to JQ1, J. Cell. Biochem. 119 (10) (2018) 8368–8377.
[29] Y.K. Tseng, et al., Effect of EGFR on SQSTM1 expression in malignancy and tumor progression of oral squamous cell carcinoma, Int. J. Mol. Sci. 22 (22) (2021).
[30] A. Iasonos, et al., How to build and interpret a nomogram for cancer prognosis, J. Clin. Oncol. 26 (8) (2008) 1364–1370.

[31] S.F. Shariat, et al., Comparison of nomograms with other methods for predicting outcomes in prostate cancer: a critical analysis of the literature, Clin. Cancer Res. 14 (14) (2008) 4400–4407.
[32] A.J. Vickers, B. Van Calster, E.W. Steyerberg, Net benefit approaches to the evaluation of prediction models, molecular markers, and diagnostic tests, Bmj 352 (2016) i6.
[33] U.M. Acuña, et al., Effects of (5Z)-7-oxozeaenol on MDA-MB-231 breast cancer cells, Anticancer Res. 32 (7) (2012) 2415–2421.
[34] H. Dan, et al., RACK1 promotes cancer progression by increasing the M2/M1 macrophage ratio via the NF-κB pathway in oral squamous cell carcinoma, Mol. Oncol. 14 (4) (2020) 795–807.
[35] D. Cihalova, F. Staud, M. Ceckova, Interactions of cyclin-dependent kinase inhibitors AT-7519, flavopiridol and SNS-032 with ABCB1, ABCG2 and ABCC1 transporters and their potential to overcome multidrug resistance in vitro, Cancer Chemother. Pharmacol. 76 (1) (2015) 105–116.
[36] O. Kujan, et al., The role of cyclin-dependent kinases in oral potentially malignant disorders and oral squamous cell carcinoma, J. Oral Pathol. Med. 48 (7) (2019) 560–565.
[37] J.H. Lee, et al., Induction of squamous cell carcinoma after MAP3K8 overexpression in murine salivry gland epithelial cells, Head Neck 41 (4) (2019) 924–929.
[38] S.H. Gohil, et al., Applying high-dimensional single-cell technologies to the analysis of cancer immunotherapy, Nat. Rev. Clin. Oncol. 18 (4) (2021) 244–256.
[39] S. Ma, et al., Identification of PTK6, via RNA sequencing analysis, as a suppressor of esophageal squamous cell carcinoma, Gastroenterology 143 (3) (2012) 675–686.e12.
[40] J. Wagner, et al., A single-cell atlas of the tumor and immune ecosystem of human breast cancer, Cell 177 (5) (2019) 1330–1345.e18.
[41] P. van Galen, et al., Single-cell RNA-seq reveals AML hierarchies relevant to disease progression and immunity, Cell 176 (6) (2019) 1265–1281.e24.
[42] T.J. Perren, et al., A phase 3 trial of bevacizumab in ovarian cancer, N. Engl. J. Med. 365 (26) (2011) 2484–2496.
[43] E. Pujade-Lauraine, et al., Olaparib tablets as maintenance therapy in patients with platinum-sensitive, relapsed ovarian cancer and a BRCA1/2 mutation (SOLO2/ENGOT-Ov21): a double-blind, randomised, placebo-controlled, phase 3 trial, Lancet Oncol. 18 (9) (2017) 1274–1284.
[44] J. Brahmer, et al., Nivolumab versus docetaxel in advanced squamous-cell non-small-cell lung cancer, N. Engl. J. Med. 373 (2) (2015) 123–135.
[45] M.H. Chien, et al., Impacts of CA9 gene polymorphisms and environmental factors on oral-cancer susceptibility and clinicopathologic characteristics in Taiwan, PLoS One 7 (12) (2012) e51051.
[46] L.B. Auzair, et al., Caveolin 1 (Cav-1) and actin-related protein 2/3 complex, subunit 1B (ARPC1B) expressions as prognostic indicators for oral squamous cell carcinoma (OSCC), Eur. Arch. Oto-Rhino-Laryngol. 273 (7) (2016) 1885–1893.